PERGAMON

Available online at www.sciencedirect.com

SCIENCE DIRECT®

International Journal of Multiphase Flow 29 (2003) 1311–1331

International Journal of Multiphase Flow

www.elsevier.com/locate/ijmulflow

Large-eddy simulation of swirling particle-laden flows in a coaxial-jet combustor

S.V. Apte [a,*], K. Mahesh [b], P. Moin [c], J.C. Oefelein [d]

[a] *Department of Mechanical Engineering, Stanford University, Bldg. 500, ME/FPC,*
488 Escondido Mall, Stanford, CA 94305-3030, USA
[b] *University of Minnesota, Minneapolis, MN 55455, USA*
[c] *Center for Turbulence Research, Stanford University, Stanford, CA 94305-3030, USA*
[d] *Sandia National Lab., Livermore, CA 94551, USA*

Received 4 February 2003; received in revised form 20 May 2003

Abstract

Large-eddy simulation (LES) of particle-laden, swirling flow in a coaxial-jet combustor is performed. A mixture of air and lightly loaded, spherical, glass-particles with a prescribed size-distribution enters the primary jet, while a swirling stream of air flows through the annulus. The incompressible, spatially filtered Navier–Stokes equations are solved on unstructured grids to compute the turbulent gas-phase. A Lagrangian formulation and an efficient particle-tracking scheme on unstructured meshes is developed to compute the dispersed phase. The particles are treated as point sources and influence the gas phase only through momentum-exchange terms. The particle-dispersion characteristics are examined in detail; in particular, the dependence of particle trajectories and residence times upon particle sizes is emphasized. The mean and turbulent quantities for the gas and particle phases are compared to experimental data and good agreement is obtained. The LES results are significantly more accurate than the Reynolds-averaged Navier–Stokes equation (RANS) predictions of the same problem. Insight into the two-phase swirling flows is obtained through the residence-times and particle velocity-diameter correlations.

© 2003 Elsevier Ltd. All rights reserved.

Keywords: Particle-laden flows; LES; Unstructured grids; Swirling flows

---

1. Introduction

Turbulent multi-phase flows are encountered in a variety of engineering applications; e.g. internal combustion engines, liquid and solid propellant rocket motors, gas-turbine aircraft engines,

---

[*] Corresponding author. Tel.: +1-650-725-1821; fax: +1-650-725-3525.
E-mail address: sapte@stanford.edu (S.V. Apte).

0301-9322/03/$ - see front matter © 2003 Elsevier Ltd. All rights reserved.

doi:10.1016/S0301-9322(03)00104-6

cyclone combustors, and biomass gasifiers (Lefebvre, 1989). The physics of such flows is extremely complex. In gas turbine combustors, for example, the liquid fuel jet undergoes primary and secondary atomization, the resulting droplets evaporate/condense and collide/coalesce, fuel and oxidizer then mix yielding spray-flames. The large amount of heat released in localized thin flame zones can often cause undesirable instabilities and acoustic resonance within the combustor.

Engineering prediction of such flows relies predominantly on the Reynolds-averaged Navier–Stokes equations (RANS). However, the large-eddy simulation (LES) technique has been convincingly shown to be superior to RANS in accurately predicting turbulent mixing and combustion dynamics (Pierce and Moin, 1998, 2001). These computations have been performed in fairly simple geometries such as the coaxial-jet combustor configuration shown in Fig. 1. The underlying numerics were therefore developed on structured grids and do not lend themselves applicable to the complex geometries of engineering gas-turbine combustors.

Recently, Mahesh et al. (2001, in preparation) have developed a numerical algorithm for high-fidelity simulations of incompressible flows on unstructured grids. A novelty of their algorithm is that it is discretely energy conserving which makes it robust at high Reynolds numbers *without numerical dissipation*. This feature was found essential to perform reliable LES in complex geometries (Mittal and Moin, 1997; Kravchenko and Moin, 1997). We have developed a Lagrangian framework for particle tracking on unstructured grids, which in conjunction with the gas-phase solver can be used for LES of particle laden flows in complex geometries. This paper describes our simulation of the turbulent, particle-laden flow in a coaxial-jet configuration of Sommerfeld and Qiu (1991, 1993) experiments which was used to validate the unstructured two phase flow solver. This work is considered an essential first step before inclusion of effects such as atomization, evaporation and combustion.

Past computational work has focused on particle–turbulence interactions in simplified geometries (Ferrante and Elghobashi, 2003; Maxey et al., 1994; Maxey and Patel, 2001; Eaton and Fessler, 1994). The effect of gas-phase velocity fluctuations on particle dispersion characteristics, preferential concentration of particles in turbulent flows, and influence of particles on the turbulence energy spectra have been investigated in depth. Considerable experimental work on turbulent particle-laden flows has also been performed (see e.g. Sommerfeld and Qiu, 1991, 1993; Kulick et al., 1994). There is evidence that the RANS can be inaccurate in predicting particle-laden flows (see e.g. Sommerfeld et al., 1992). There has been only one prior LES in a coaxial-jet

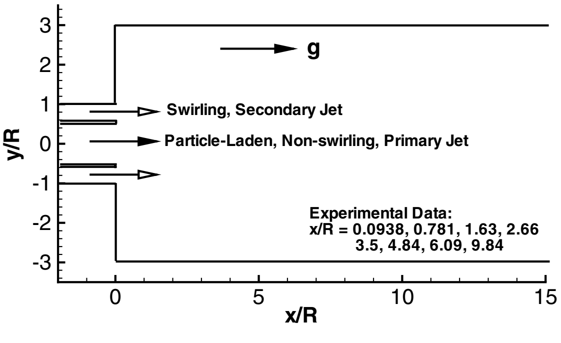

Fig. 1. Schematic of the swirling, coaxial-jet combustor.

combustor geometry (Oefelein, 1999). However, Oefelein used a body-fitted, structured-grid solver to develop particle-tracking methodology for LES; as a result his approach is limited to simplified combustor geometries. This Lagrangian framework was modified and implemented into the present unstructured LES code. To the best of our knowledge, the work described in this paper represents the first LES of turbulent particle-laden flows using a methodology that is directly applicable to complex engineering configurations.

The paper is organized as follows. Section 2 provides a brief overview of the gas and particle phase equations. The particle-tracking and interpolation algorithms on unstructured grids are presented in Section 2.2.1. Section 3 presents results from the LES. A detailed comparison with experiments for both phases is shown. The residence times for different size particles is estimated and compared with numerical and analytical estimates. Also, computed correlations between particle velocity and diameter size are compared to experiment.

2. Theoretical formulation

The governing equations used for the gaseous and dispersed phases are described briefly. Two-way interactions between the gas and particle phases are included; however, for the small particle loadings used in the present simulation, the effect of particle volume on the gas-phase is neglected. The particles are treated as point-sources and influence the gas-phase only through momentum-exchange terms. The particle-tracking and interpolation schemes are described in detail.

2.1. Gas-phase

The three-dimensional, incompressible, filtered Navier–Stokes equations are solved on unstructured grids with arbitrary elements. These equations are written as

$$\frac{\partial \bar{u}_i}{\partial t} + \frac{\partial \bar{u}_i \bar{u}_j}{\partial x_j} = -\frac{\partial \phi}{\partial x_i} + \frac{1}{Re_{\mathrm{ref}}} \frac{\partial^2 \bar{u}_i}{\partial x_j \partial x_j} - \frac{\partial q_{ij}}{\partial x_j} + \overline{\dot{S}_i}, \tag{1}$$

where q_{ij} denotes the anisotropic part of the sub-grid scale stress tensor, $\overline{u_i u_j} - \bar{u}_i \bar{u}_j$, and the overbar indicates filtered variables. The dynamic Smagorinsky model by Germano et al. (1991) is used for q_{ij}.

The source-term $\overline{\dot{S}_i}$ in the momentum-equations represent the ‘two-way’ coupling between the gas and particle-phases and is given by

$$\overline{\dot{S}_i} = -\frac{1}{V_{\mathrm{cv}}} \sum_k \frac{\rho_{\mathrm{p}}^k}{\rho_{\mathrm{ref}}} V_{\mathrm{p}}^k \frac{\mathrm{d}u_{\mathrm{p}i}^k}{\mathrm{d}t}, \tag{2}$$

where the subscript p stands for the particle phase. Eq. (1) is non-dimensionalized by the reference length, velocity, and density scales, L_{ref}, U_{ref}, ρ_{ref}, respectively. The reference Reynolds number is defined as $Re_{\mathrm{ref}} = \rho_{\mathrm{ref}} L_{\mathrm{ref}} U_{\mathrm{ref}} / \mu_{\mathrm{ref}}$. Here, V_{cv} and $V_{\mathrm{p}}^k = \frac{\pi}{6} d_{\mathrm{p}}^{k^3}$ are the volumes of the computational cell and particle k, respectively. The $\sum_k$ is over all particles in a computational control volume.

An energy-conserving scheme for unstructured, arbitrarily shaped grid elements (Mahesh et al., 2000, 2001, in preparation) is used to solve the gas-phase equations. The velocity and pressure are stored at the centroids of the volumes. The cell-centered velocities are advanced in a predictor step such that the kinetic energy is conserved. The predicted velocities are interpolated to the faces and then projected. Projection yields the pressure potential at the cell-centers, and its gradient is used to correct the cell and face-normal velocities. A novel discretization scheme for the pressure gradient was developed by Mahesh et al. (in preparation) to provide robustness *without numerical dissipation* on grids with rapidly varying elements. This algorithm was found to be imperative to perform LES at high Reynolds number in realistic combustor geometries. This formulation by Mahesh et al. (in preparation) has been shown to provide very good results for both simple and complex geometries and is used in the present simulation.

2.2. Particle-phase

The particle motion is simulated using the Basset–Boussinesq–Oseen (BBO) equations (Crowe et al., 1998). It is assumed that the density of the particle is much larger than that of the fluid ($\rho_p/\rho_f \sim 10^3$), collisions among particles are negligible, particle-size is small compared to the turbulence integral length scale, and that the effect of shear on particle motion is negligible. The high value of ρ_p/ρ_f implies that density ratio implies that the Basset force and the added mass term are small and are therefore neglected. The effect of shear on the particles is generate the Saffman lift force. The ratio of the lift to drag force is given by $F_{\text{Saff}}/F_{\text{drag}} \sim d_p^2 (\mathrm{d}u/\mathrm{d}y)^{1/2}/\nu$ and is dependent on the shear rate and particle diameter. For particles with small diameter and low inertia this force can be neglected in comparison to the drag force (Crowe et al., 1998). Under these assumptions, the Lagrangian equations governing the particle motions become:

$$\frac{\mathrm{d}\mathbf{x}_p}{\mathrm{d}t} = \mathbf{u}_p, \tag{3}$$

$$\frac{\mathrm{d}\mathbf{u}_p}{\mathrm{d}t} = \frac{f}{St_p}(\mathbf{u} - \mathbf{u}_p) + \frac{L_{\text{ref}}}{U_{\text{ref}}^2}\mathbf{g}, \tag{4}$$

where f is the drag coefficient and St_p the particle Stokes number defined as

$$St_p = \frac{\tau_p}{\tau_f} = \frac{(\rho_p^* d_p^{*2})/(18\mu_{\text{ref}})}{(L_{\text{ref}}/U_{\text{ref}})} = \frac{1}{18}\rho_p d_p^2 Re_{\text{ref}}. \tag{5}$$

The mean flow time scale τ_f appears in Eq. (5) as the gas and particle-phase equations are normalized by the same reference scales. The superscript $*$ represents dimensional quantities. The drag coefficient f is modeled as function of particle Reynolds number, $Re_p = d_p Re_{\text{ref}} |\mathbf{u} - \mathbf{u}_p|$. For particle Reynolds number up to 800, Schiller and Naumann (see Crowe et al., 1998) propose the non-linear correlation

$$f = (1 + aRe_p^b). \tag{6}$$

This yields a drag coefficient with less than 5% deviation from the standard drag curve for $a = 0.15$, $b = 0.687$. The ratio St_p/f is a non-dimensional particle relaxation time,

$$\frac{\tau_r}{\tau_f} = \frac{St_p}{f}. \tag{7}$$

The gas-phase velocity, **u**, in Eqs. (3) and (4) is computed at individual particle locations within a control volume using a generalized, tri-linear interpolation scheme for arbitrary shaped elements. Introducing higher order accurate interpolation is straightforward; however, it was found that tri-linear interpolation is sufficient to represent the gas-phase velocity field at particle locations. Note that we have neglected the direct effect of sub-grid scale (sgs) fluctuations on the particle motion. The direct sgs effect is determined by the time scale of the sgs fluctuations and their energy content. These effects will be small when the sgs time scale is large compared to the particle relaxation time and the energy content is low compared to the resolved scale turbulent kinetic energy. Section 3.3.1 provides a posteriori estimates to suggest that the direct sgs effects are negligible for the present flow.

Eqs. (3) and (4) are integrated using a fourth-order Runge–Kutta time-stepping algorithm. After obtaining the new particle positions, the particles are relocated, particles that cross inter-processor boundaries are duly transferred, boundary conditions on particles crossing boundaries are applied, source terms in the gas-phase equation are computed, and the computation is further advanced. Solving these Lagrangian equations thus requires addressing the following key issues: (i) efficient search and location of particles on an unstructured grid, (ii) interpolation of gas-phase properties to the particle location for arbitrarily shaped control volumes, (iii) inter-processor particle transfer.

2.2.1. Locating particles in elements of arbitrary shape

Locating particles in a generalized-coordinate structured code is straightforward since the physical coordinates can be transformed into a uniform computational space. This is not the case for unstructured grids. Westermann (1992) describes several approaches to locate particles in particle-in-cell codes. Two such techniques are described below.

One approach to determine whether a particle lies inside a control volume is based on the calculation of partial volumes. The nodes of the control volume are joined to the particle location, and the volumes of the resulting sub-cells are compared to that of the control volume. If the particle lies inside the control volume, the sum of the sub-cell volumes will be equal to the total volume. However, this approach was found to fail drastically for highly skewed meshes due to round-off inaccuracies in the computation of partial volumes.

The second approach projects the particle location onto the faces of the control volume and compares these vectors with outward face-normals for all faces. If the particle lies within the cell, the projected vectors point the same way as the outward face-normals. This technique is found to be very accurate even for highly skewed elements. A search algorithm is then required to efficiently select the control volume to which the criterion should be applied.

2.2.2. Search algorithms for particles on unstructured grids

Three approaches were examined and are termed as the brute-force, modified brute-force and known-vicinity algorithms, respectively. The brute-force approach simply loops over all the elements of the grid and applies the localization criterion described above. As expected, it is extremely slow for a large number of particles, as is the case even for coarse LES. The modified brute-force approach evaluates the closest point of the mesh to the particle location and only considers the elements surrounding that point. Should this attempt (which in general is very successful) fail, the elements surrounding all the close points are considered. If this also fails for some pathological cases (Lohner, 1995), the search region is enlarged or the brute force method is applied. This modified approach is found effective to initialize particles, and as a fallback position for more refined algorithms.

Given a good initial guess for a particle location, the known-vicinity algorithm out performs all others (Lohner, 1995). Particle location at earlier time-steps provide a very good initial guess in LES. Knowing the initial and final location of the particle, this algorithm searches in the direction of the particle motion until it is relocated (Fig. 2). The neighbor-to-neighbor search is extremely efficient if the particle is located within 10–15 attempts, which is usually the case for 95% of the particles in present simulations. If this algorithm fails, we fallback to the 'modified-brute force' method to locate the particle. A combination of these two algorithms is found highly efficient and robust for complex geometries and hybrid meshes encountered in realistic combustor geometries. A similar approach was also applied by Li and Modest (2001) to perform hybrid finite volume/PDF-Monte Carlo simulations implying a wide range of potential applications utilizing this scheme.

The known-vicinity algorithm is compared to the modified-brute force method in Fig. 2. Two cases are considered: (i) the grid is fixed, and the particles are displaced by 2–3 cell-sizes in all three

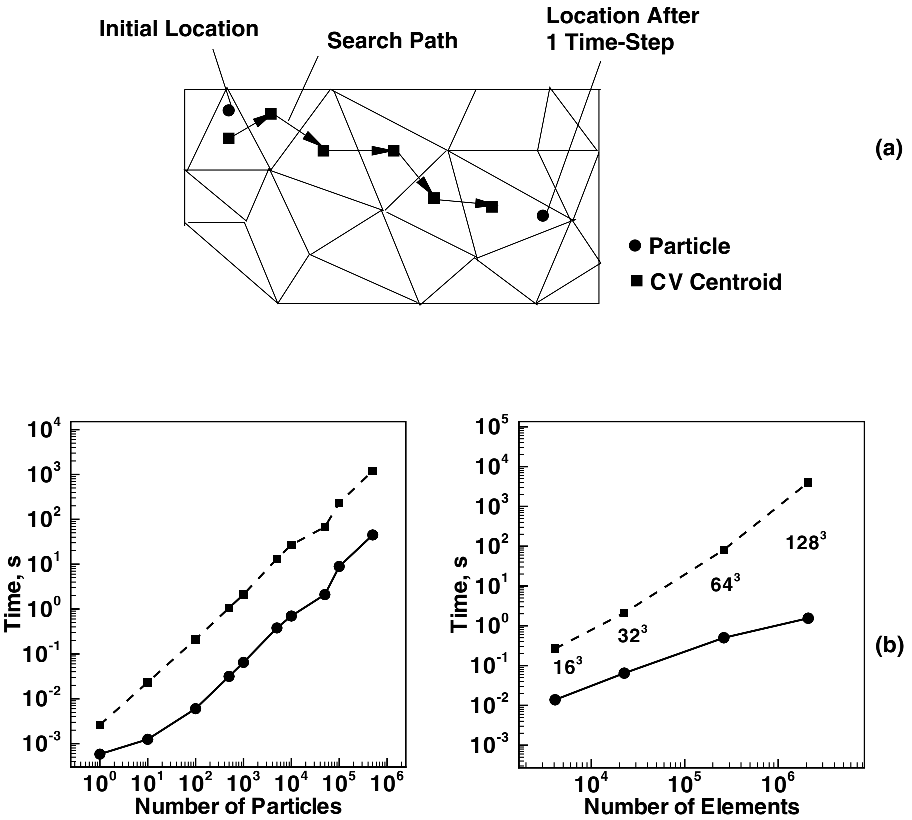

Fig. 2. (a) Schematic of the known-vicinity algorithm to track particle positions on unstructured grids. (b) Comparison of the modified brute force and known vicinity search algorithms, (—) known-vicinity, (- - -) modified brute force.

coordinate directions, (ii) the number of particles is fixed ($\sim$1000) and the number of elements per processor is increased. The known-vicinity approach is seen to be noticeably better than the modified brute-force. Note that these comparisons were performed on a single processor of an Origin 2000 for a cubic box with tetrahedral elements.

2.2.3. Interpolation of gas-phase properties

The gas-phase properties, such as velocity vector, are needed at the particle locations in Eqs. (3) and (4). These are obtained by interpolation from the gas-phase velocities at the centroids of the cell, which the particle belongs to and its neighbors. For complex combustor geometries, highly skewed, 'bad' grid elements are inevitable. A robust interpolation algorithm is necessary for Lagrangian computations on such grids, where the search algorithm may give an approximate cell location. Additionally, a control volume may have variable number of neighbors depending on its shape. Hence, a least-squares interpolation technique is used to linearly interpolate the gas-phase properties to the particle location. For the present second-order gas-phase solver, first-order interpolation of gas-phase properties is found to be sufficient to accurately resolve the particle motions. This is a robust interpolation scheme which also allows for extrapolation in case the search routines predict an approximated cell location for highly skewed meshes and/or arbitrary and complex domain decompositions.

After solving the particle equations, the particles that cross interprocessor boundaries are assigned to the ghost control volumes of the gas-phase solver, and then passed across processors. They are then relocated by utilizing the search routines of the new processors, and the number of particles per processor is continually adjusted and checked for mass conservation. This efficient parallelization for Lagrangian formulation allows us to use arbitrary domain-decomposition and thus better distribute the computational load among the processors.

2.3. Boundary conditions

For the gas-phase, the mass-flow rate at the inlet is kept constant. For a given mass-flow rate, the turbulent velocity components in the primary and annular pipe sections are obtained using the body-force technique developed by Pierce and Moin (1998). This inflow data over several flow through times is generated a priori and read at each time step to specify the velocity components at the inlet. Convective boundary conditions are applied at the exit section by conserving the global mass flow rate through the combustor. No-slip conditions are enforced at the walls. In this work, we use the dynamic sub-grid model (Germano et al., 1991) which can be integrated all the way to the wall. The wall is therefore resolved and no wall-model is used.

The mass-flow rate and inlet particle diameter distribution determines the number of particles to be injected per time step. The pdf for particle diameter distribution is matched with the experimental data by using an upper limit log-normal distribution in order to match the mean number density and variance with the experimental data. The upper limit log-normal distribution is given as,

$$f(d_{\mathrm{p}}) = \frac{1}{\sqrt{2\pi}\sigma_0}\frac{1}{a_0 d_{\mathrm{p}}}\exp\left[-\left(\frac{\log d_{\mathrm{p}}^{+} - \log D_{\mathrm{nm}}^{+}}{\sigma_0}\right)^2\right], \tag{8}$$

where $d_\mathrm{p}^+ = d_\mathrm{p}^*/(d_\mathrm{p}^{*\,\max} - d_\mathrm{p}^*)$, and $D_\mathrm{nm}^+ = D_\mathrm{nm}^*/(d_\mathrm{p}^{*\,\max} - D_\mathrm{nm}^*)$ are the normalized particle diameters, $d_\mathrm{p}^{*\,\max}$ is the upper limit of particle diameter, D_nm^* the mean, σ_0^2 the variance, and a_0 a factor used to normalize the pdf. In the present work, $d_\mathrm{p}^{*\,\max} = 125$ μm, $D_\mathrm{nm}^* = 48.0$ μm, and $\sigma_0 = 0.6$, respectively. This gives the mean expectation of diameter as 45.5 μm. This expression was derived to analytically fit the experimental data acquired by Sommerfeld.

The particle diameter is sampled from the above distribution function, a particle location is selected with uniform distribution over the inlet face, and the velocity of the particle is assigned equal to the gas-phase velocity at the particle location. particle–wall interactions are modeled using Snell's law of specular reflection (Modest, 1993). The direction of particle reflection, $\hat{\mathbf{s}}_\mathrm{r}$ is determined from the incident direction, $\hat{\mathbf{s}}_\mathrm{i}$, and the inward face-normal at the wall surface, $\hat{\mathbf{n}}$ as

$$\hat{\mathbf{s}}_\mathrm{r} = \hat{\mathbf{s}}_\mathrm{i} + 2|\hat{\mathbf{s}}_\mathrm{i} \cdot \hat{\mathbf{n}}|\hat{\mathbf{n}}. \tag{9}$$

The velocity direction is also modified according to (9). Particles leaving the outflow section are simply deleted.

3. Results and discussion

3.1. Computational domain, grid generation and flow conditions

Fig. 1 shows a schematic of the coaxial combustor investigated by Sommerfeld and Qiu (1991, 1993). The chamber consists of central core (primary) and annular (secondary) jets discharging into a cylindrical test section with sudden expansion. The primary jet has a radius of 16 mm and is laden with glass beads with a mean number diameter (D_{10}) of 45 μm distributed between 10 and 120 μm. The secondary annular jet has a swirling azimuthal velocity and extends over the radial interval of 19–32 mm. The outer radius of the annulus ($R = 32$ mm) is taken as the reference length scale (L_ref) with which the computational domain and flow parameters are scaled. The whole test-section is 960 mm long, is oriented vertically with gravity acting in the direction of the flow and is connected to a stagnation chamber of length 640 mm and radius 288 mm. The numerical simulations of turbulent swirling flows in coaxial combustors by Pierce and Moin (2001) indicate that the existence of a stagnation chamber downstream greatly alters the location of recirculation zones upstream. The stagnation chamber is therefore included in the present simulation.

Fig. 3 shows the unstructured grid used. The computational domain is divided in $\sim 1.6 \times 10^6$ hexahedral volumes, with $\sim 0.9 \times 10^6$ elements clustered in the first half of the test section. Approximately 96 grid points are used in the azimuthal direction. As shown in Fig. 3, the central region of the primary jet consists of a square mesh which eliminates the coordinate singularity point commonly observed in axisymmetric structured grids near the centerline. This is important for the known-vicinity search algorithm to work properly if the particles cross the centerline in the radial direction. For grids with a singular point at the center the search path in the known-vicinity algorithm is circular and makes large number of attempts, rendering it inefficient. A modified brute-force method would have to be used in such cases. With the present grid this deficiency is eliminated. The smallest grid spacing is ~ 32 μm near the walls and in the shear layers with steep velocity gradients close to the annular inlet into the test-section. For the present swirling flowfield,

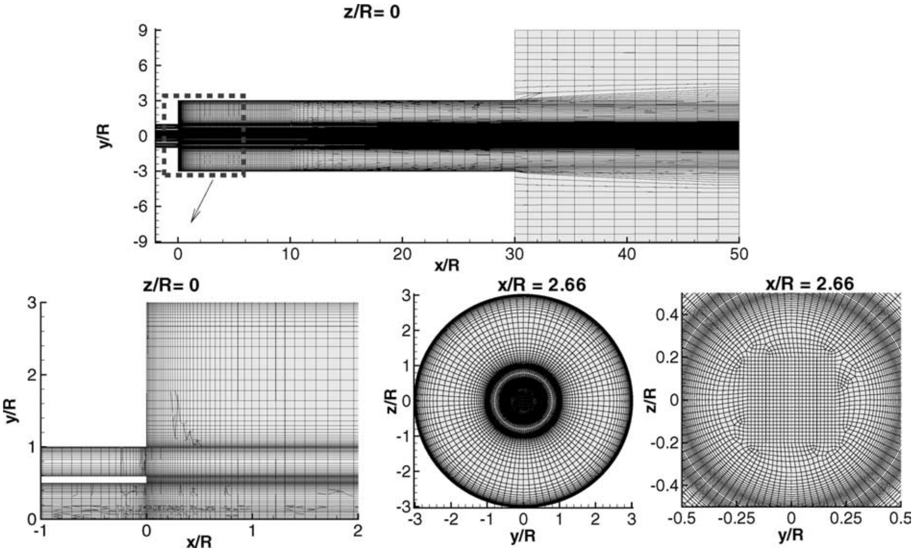

Fig. 3. Computational domain and grid distribution.

Table 1
Flow conditions and particle properties used in the Sommerfeld and Qiu (1991) experiments

Gas phase (air)		Particle phase (glass)	
Flow rate in primary jet, g/s	9.9	Loading ratio in primary jet	0.034
Flow rate in secondary jet, g/s	38.3	Flow rate, g/s	0.34
Inlet Reynolds number	26,200	Density ratio, ρ_p/ρ_f	2152
Swirl number	0.47		

the dominant flow mechanism of interest is the behavior of the particles in the recirculation zones. To accurately resolve these zones it is necessary to resolve wall effects within the axial and annular inlet sections so that the flow dynamics within the shear layers just downstream evolve correctly. The flow is governed by the swirling motion giving rise to rapid spreading and reattachment of the shear layers. The wall layers on the horizontal walls of the chamber are not critical and the resolution in this region is specified such that the reattachment point is correctly resolved.

Table 1 provides the flow conditions for the gas and particle phases. The particle loading ratio of 0.034 is too small to have dense clusters of particles, and the particle–particle interactions are neglected in the present simulation. The reference velocity, $U_{\mathrm{ref}} = 12.89$ m/s is obtained based on the total volume flow rate and cross-sectional area of the inlet section. This gives an inlet Reynolds number of $Re_{\mathrm{ref}} = 26{,}200$. Fig. 4 shows the particle size distribution in the primary jet given by Eq. (8). The y–z location of the primary jet is chosen randomly and a particular diameter is assigned based on the distribution shown in Fig. 4. The total number of particles injected per time step is determined based on the mass-flow rate and varies between 10 and 20 for a non-dimensional time-step of 1.2×10^{-3}. It should be noted that, in the present LES computation, *each particle is tracked*; this yields around 1.1×10^{6} particles in the domain with two-way coupling applied between the gas and particle phases. In contrast, RANS computations (Sommerfeld et al.,

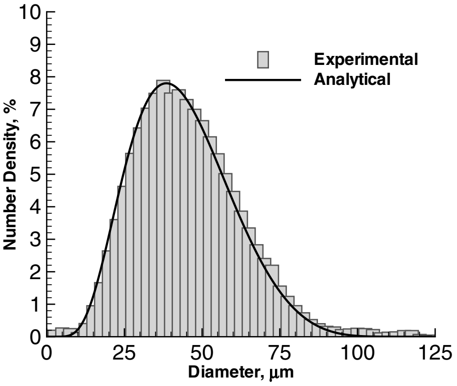

Fig. 4. Particle diameter distribution.

1992) typically cluster particles of certain size-classes to form 'parcels' thus keeping the number of computational particles small (~1000–5000). This, however, is not suitable for dynamic representation of dispersed phase in the context of LES.

The computational domain is partitioned into 96 sub-domains and assigned to individual processors for parallel computation. The domain-decomposition is based on the Eulerian grid which is fine close to the exit of the primary and secondary jets distributing equal number of control volumes per processor. Addition of particle-phase, however, may imbalance the computational load per processor as the processor carrying more particles may lag behind others. For the present computation of small particle-loading ratio, this effect is found to be negligible as the total overload due to million Lagrangian particles is around 20–30%. The computations were performed on the IBM SP at the San Diego Supercomputing Center and took around 150 CPU-hours for one flow-through time on 96 processors.

3.2. Validation of Eulerian–Lagrangian formulation

The global characteristics of the recirculation zones, mean and root-mean-square (rms) of velocity components of both phases, particle size distributions, and particle dispersion characteristics are compared to Sommerfeld and Qiu's (1991) experiments.

3.2.1. Global characteristics

Fig. 5 shows the instantaneous contours of axial velocity at cross-sections $z = 0$, $x = 0.786$, $x = 1.63$, and $x = 2.66$, respectively. The corresponding particle locations for 1 mm cross-sections are superimposed on the turbulent velocity field. The size of the circles scales with the actual diameter of the particles. The expansion of the swirling jet, central and secondary recirculation regions are clearly visible. Close to the entrance of the test-section at $x = 0$, particles are concentrated in the central core region. Particles are injected with the same velocities as the gas-phase at the inlet, however, majority of them do not follow the rapid expansion and deceleration of the gas jets. These particles are convected downstream and spread in the radial and azimuthal directions, some of them are trapped in the central recirculation region. Particles tend to have higher

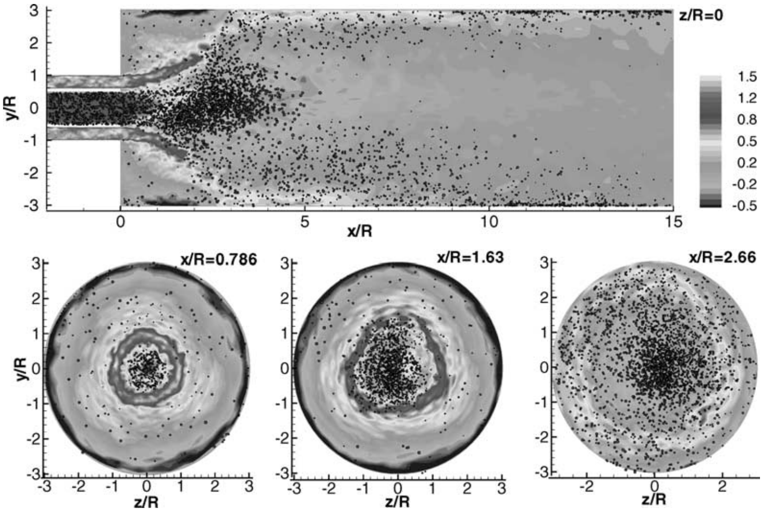

Fig. 5. Cross-section of the test section and particles superposed on contours of instantaneous axial velocity. Conditions correspond to the experiment by Sommerfeld and Qiu (1991).

velocities in the core region, penetrate the central recirculation region, move against the gas-phase flow till they are decelerated to zero axial velocity. These particles then change their direction, and are thrown radially outwards by the centrifugal action.

Heavier particles penetrate the recirculation bubble the most because of their larger inertia. These particles escape through the exit section at around $x/R = 15$. Particle trajectories beyond this axial location are not simulated owing to the lack of experimental data far downstream. An estimate of residence time is also obtained from these numerical simulations for particles belonging to different size-classes. The primary and secondary recirculation zones with cores centered at $(x/R, r/R)$ of $(3.7, 2.0)$ and $(1.4, 2.4)$, respectively, agree very well with the experimental values. The reattachment point for the swirling jet is located at $(2.56, 3.0)$.

3.2.2. Gas-phase statistics

Fig. 6a–c show the radial variations of azimuthally averaged axial, swirl, and radial components of the mean velocity at various axial locations compared with the experimental data. The agreement of all the velocity components with the experiments is very good at all test-sections. The large radial velocity at $x/R = 0.786$ indicates the strong spreading of the inlet jets due to the swirl. The rms fluctuations of the velocity components also show similar good agreement (Fig. 6d–f). Note that the level of agreement is noticeably better than RANS predictions of the same problem (see, Figs. 6–9 in Sommerfeld et al., 1992). This shows the superiority of LES in accurately predicting particle dispersion and also confirms the accuracy of the present numerical approach on unstructured grids.

3.2.3. Particle-phase statistics

Fig. 7a–f shows the particle mean velocity distributions and the rms fluctuations. The mean and rms values for particle properties are obtained by performing ensemble averages as the particles

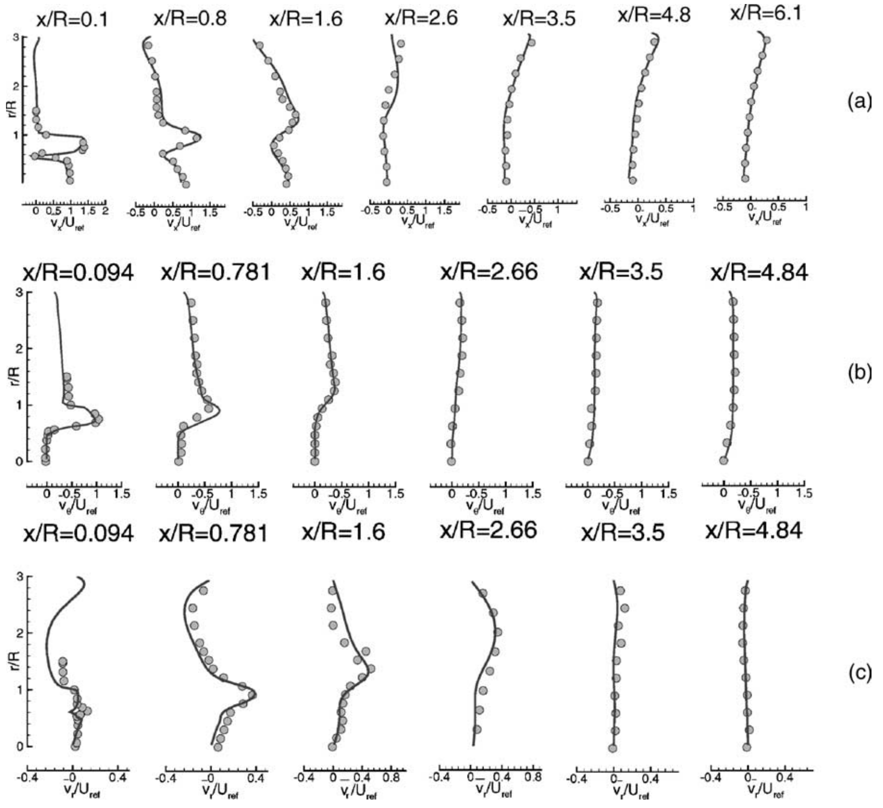

Fig. 6. Comparison of gas-phase properties between LES (—) and experiment (○, Sommerfeld and Qiu, 1991) for swirling flow in a coaxial combustor: (a) mean axial velocity, (b) mean swirl velocity, (c) mean radial velocity, (d) rms of axial velocity, (e) rms of swirl velocity, (f) rms of radial velocity.

cross the control volumes in the computational domain. The averages are obtained over 3–4 flow through times in order to have independent samples. The ensemble means are then averaged azimuthally. This again shows very good agreement with the experimental data confirming that the particle–turbulence interactions are correctly captured by the LES. Accurate predictions of the mean and rms values of the particle velocities represents strong evidence of the accuracy of the present numerical scheme for Lagrangian particle tracking on unstructured grids. Compared to the gas-phase profiles, the mean particle velocities in the core region are higher due to the larger inertia of the heavy particles.

Fig. 8a and b shows the evolution of the mean and rms number diameter (D_{10}) at various axial locations in the flowfield compared with the experiment. Tracking individual trajectories of around million particles in the domain as opposed to the parcels-approach is well justified by the accuracy of the present result (for results using parcels-approach see Sommerfeld et al., 1992). The mean number diameter is around 45 μm in the upstream core region. It increases along the center line further downstream indicating that only large particles penetrate the central recirculation bubble to a large extent before they are thrown outwards by swirling motion. The mean diameter also decreases with increase in radius. Smaller particles, with less inertia are basically carried with

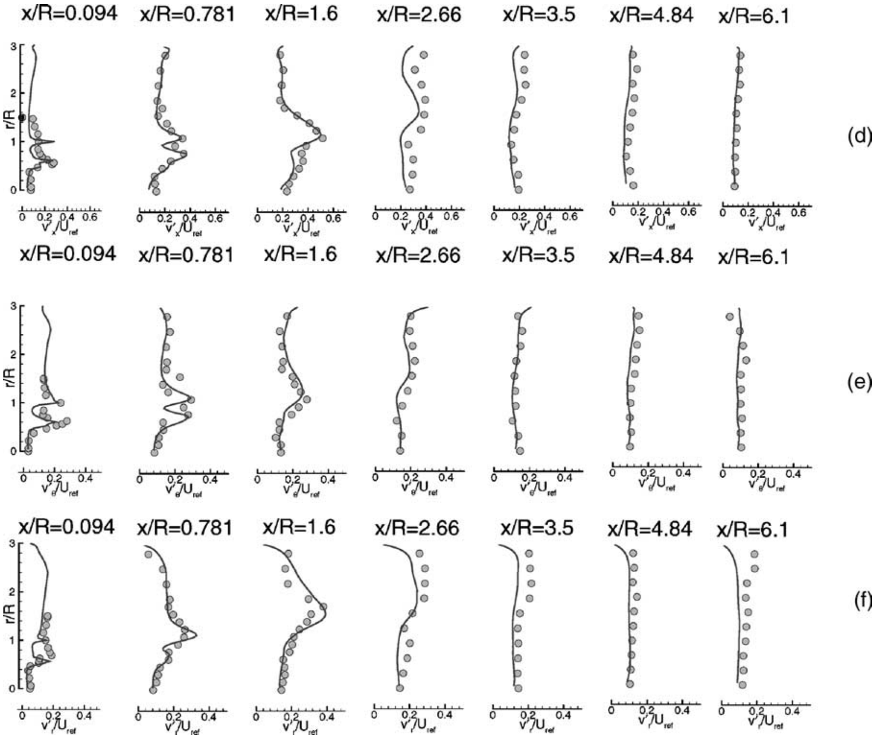

Fig. 6 (*continued*)

the gas-phase without large relative velocities and appear on the outer-edge of the recirculation zone.

3.3. Particle dispersion characteristics

3.3.1. Particle trajectories

Particle trajectories of different size-classes exposed to the same gas-phase flowfield are computed numerically and are shown in Fig. 9. The trajectories were obtained by injecting 20,000 tagged particles of each size class at $x/R = -2$, $z/R = 0$, and y/R uniformly distributed over the radius of the primary jet. The particles were injected with velocity equal to the local gas-phase velocity. It is clearly seen that particles with diameters less than 80 μm decelerate to zero velocity within the central recirculation bubble. Their larger inertia causes large diameter particles to penetrate more into the recirculation zone before coming to a halt. These particles then accelerate towards the inlet and are transported radially outwards by the centrifugal forces. The particles then exit the region of reverse flow and are entrained by the annular jet which transports them downstream with swirling motion and multiple reflections off the wall. Particles with $d_p > 100$ μm tend to penetrate the central recirculation bubble completely without coming to halt, whereas particles with $d_p < 30$ μm follow the gas-phase flow. Fig. 9 shows the benefits of LES over RANS in predicting particle dispersion. Note that the particle trajectories for all diameter classes agree

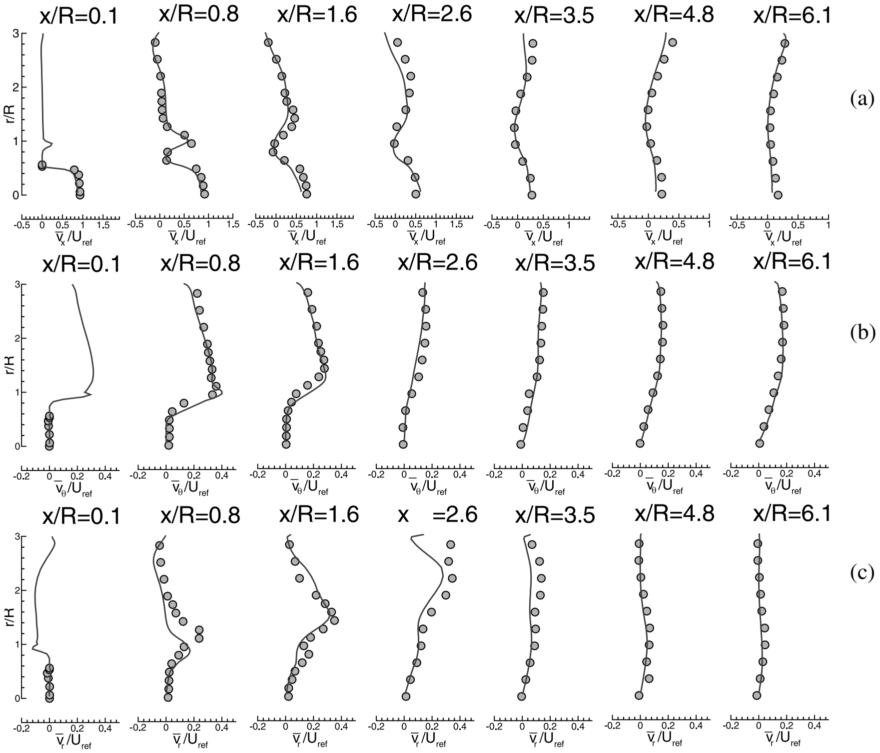

Fig. 7. Comparison of particle phase properties between LES (—) and experiment (○, Sommerfeld and Qiu, 1991) for swirling flow in a coaxial combustor: (a) mean axial velocity, (b) mean swirl velocity, (c) mean radial velocity, (d) rms of axial velocity, (e) rms of swirl velocity, (f) rms of radial velocity.

well with the experimental data. In contrast, predictions by Sommerfeld et al. (1992) using RANS-type closures show negligible dispersion of particles within the combustor unless explicit particle-dispersion models are used.

We have neglected the direct effect of the sgs fluctuations on particle dispersion. However, note that the particles *do feel* the sub-grid scales through the sub-grid model that affects the resolved velocity field. The direct effect of the sub-grid scales is expected to be important when the sub-grid scale energy is significant as compared to the resolved scales and the time scales of the sgs fluctuations are comparable to the particle relaxation time, τ_r. As shown in Fig. 9, these assumptions are tested by comparison to Sommerfeld's experiments. The level of agreement suggests that our assumptions are justified for this flow and for the quantities being compared. A posteriori estimate of the sgs energy content in the shear dominated region ($0 < x/R < 2$, $0 < r/R < 2$) shows that only 10% of the total turbulent kinetic energy is present in the sub-grid scales. Also the estimated Kolmogorov and Taylor microscale in this region are around 0.04 and 1.5 mm, respectively. As seen from Fig. 9, the mean size of particles observed in this region is around 30–40 μm. The corresponding dimensionless Kolmogorov and Taylor time scales are 5–15% of the characteristic reference time scale ($\tau_f = L_{ref}/U_{ref}$). The particle relaxation time, τ_r in this region ranges between 10% and 50% of τ_f. Although direct effects of the sgs fluctuations are not important in our

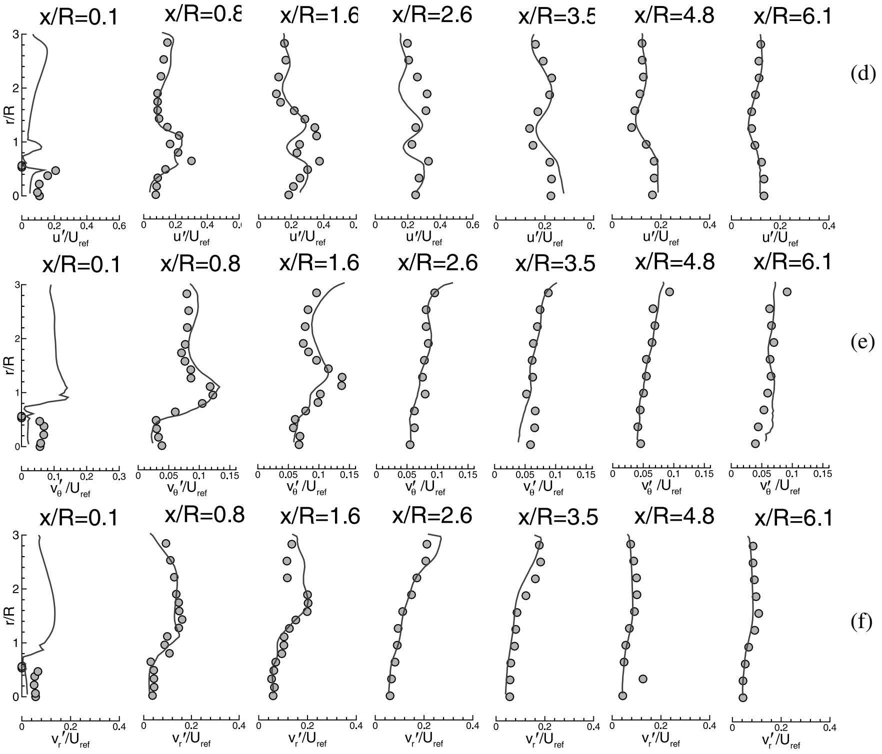

Fig. 7 (*continued*)

computations, they could be significant in situations with higher particle loadings or near-wall regions where particle number density and the sgs energy content tends to be high.

3.3.2. Particle response characteristics

As suggested by Sommerfeld et al. (1992), the particle response characteristics in a swirling flow can be characterized by time and length-scale ratios, $S_1 = \tau_p/\tau_s$, $S_2 = \Delta l/L_{rec}$. S_1 represents the ratio of the particle response time τ_p (given by Eq. (5)) to the time required for the particle to travel from the primary jet exit to the stagnation point of the central recirculation bubble τ_s. The central recirculation bubble is located around 75 mm downstream of the primary jet exit and is identified by tracking the particles till the axial gas-phase velocity first becomes negative. S_1 is then computed by averaging the particle response times and τ_s for the 20,000 tagged particles of each size class. S_2 is the ratio of the length, Δl, traversed by the particle starting from its entry into the recirculation zone till it comes to rest, Δl, to the length of the recirculation bubble, L_{rec}. This ratio can also be approximately represented by the ratio of the distance traveled by the particle within the recirculation zone, $\Delta l = \int_0^{t_{p0}} u_p\,dt$, to the total length of the reverse flow regime, $L_{rec} \sim 255$ mm. Only those particles which enter the reverse flow regime are taken into account.

Sommerfeld et al. (1992) provided analytical estimates of S_1 and S_2 by assuming one-dimensional low-Reynolds number Stokes flow ($f = 1$), neglecting gravity, and approximating the axial

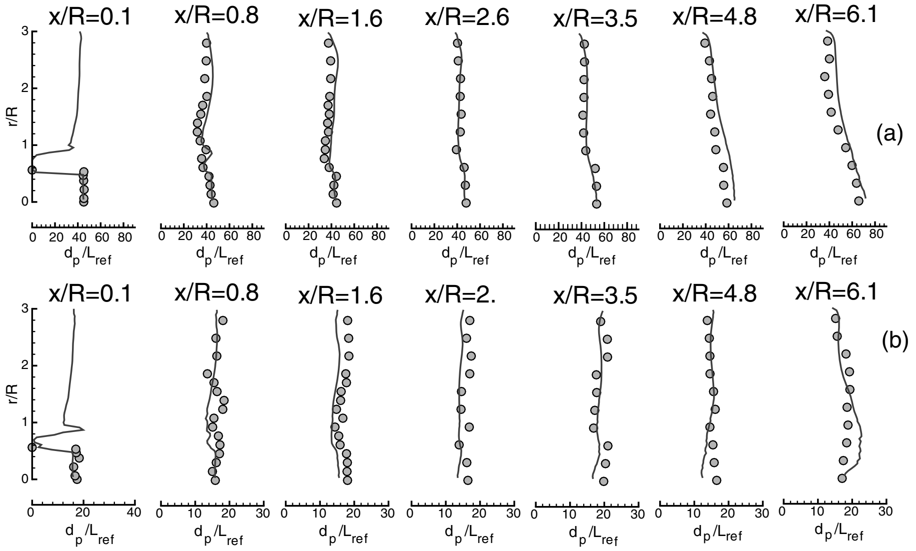

Fig. 8. Comparison of particle diameter between LES (—) and experiment (∘, Sommerfeld and Qiu, 1991) for swirling flow in a coaxial combustor: (a) mean number diameter, (b) rms number diameter.

gas-phase velocity in the recirculation zone by a constant, (u_g). With these assumptions, Eq. (6) can be written in dimensional form as

$$\frac{\mathrm{d}u_p}{\mathrm{d}t} = \frac{1}{\tau_p}(u_g - u_p). \tag{10}$$

Integrating Eq. (10) up to time $t = \Delta t$ we get

$$u_p = u_g - (u_g - U_{ps}) \exp\left(\frac{-\Delta t}{\tau_p}\right). \tag{11}$$

Starting at the tip of the recirculation bubble, the time required for the particle to come to rest (t_{p0}) is given as

$$t_{p0} = \tau_p \ln\left(\frac{u_g - U_{ps}}{u_g}\right). \tag{12}$$

The distance traveled by the particle within the recirculation zone before coming to rest is $\Delta l = \int_0^{t_{p0}} u_p \, \mathrm{d}t$. S_1 and S_2 are estimated by using the maximum value of negative gas-phase velocity in the recirculation regime, $(u_g \approx -2.1$ m/s) and computing U_{ps} from the particle velocity at the primary jet exit $U_{p0} \approx 12.5$ m/s.

Fig. 10 shows the variation of these two parameters with respect to the particle size. Also plotted are the analytical estimates obtained by Sommerfeld et al. (1992). The ratio $S_1 < 1$ implies that the particle response times are small and the particles are basically carried by the gas-phase with small relative velocity between them. Fig. 10 shows that for $D_p < 30$ μm the particles follow the gas-phase and respond to the flow reversal as soon as they enter the recirculation zone. Very small particles may move along the edge of the recirculation bubble without entering it. Particles

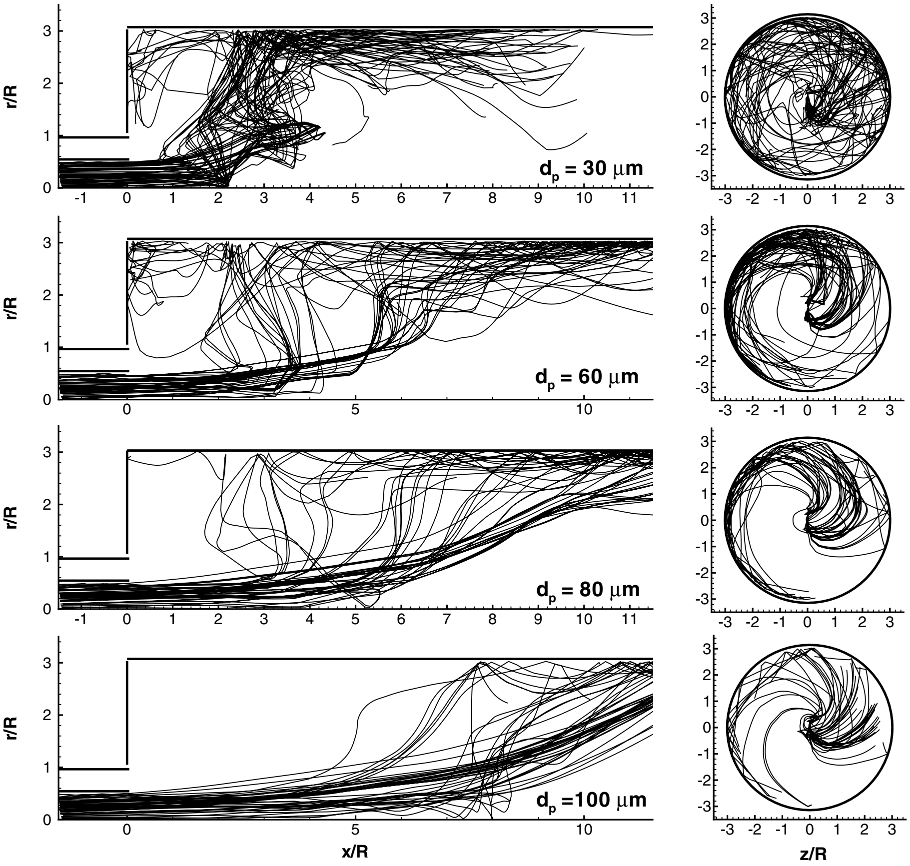

Fig. 9. Particle trajectories for different size classes.

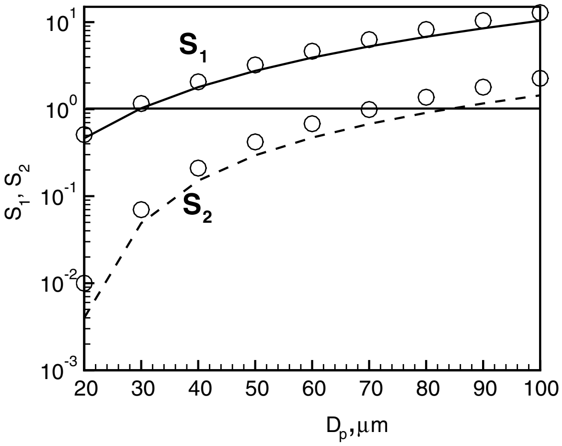

Fig. 10. Particle response characteristics, (—, - - - present), (○, Analytical estimates by Sommerfeld and Qiu, 1991).

with $S_1 > 1$ have more inertia and exhibit larger axial velocities at the stagnation point and are forced into the recirculation zone. Larger size particles penetrate more into the recirculation zone and are decelerated slowly. For $S_2 > 1$, the particles have very large inertia and penetrate the recirculation zone completely as shown by particles with $D_p > 80$ μm. This is also evident from the trajectories shown in Fig. 9. Particles with $D_p = 100$ μm tend to pass through the reverse flow regime without decelerating to zero axial velocity. These particles however, are thrown radially outwards further downstream because of the swirling motion.

3.3.3. Particle residence times

An estimate of the residence time in $0 < x/R < 12$ is shown in Fig. 11a. The residence time is normalized by the time required by the particle to come to rest, t_{p0} given in Eq. (12). The residence time decreases with increasing particle size. This is because small size particles swirl along the periphery of the test-section before exiting the computational domain, which increases their residence time. Also shown in Fig. 11 is the residence time in the central recirculation region normalized by t_{p0}. This ratio becomes less than unity for particle sizes $d_p > 80$ μm and indicates

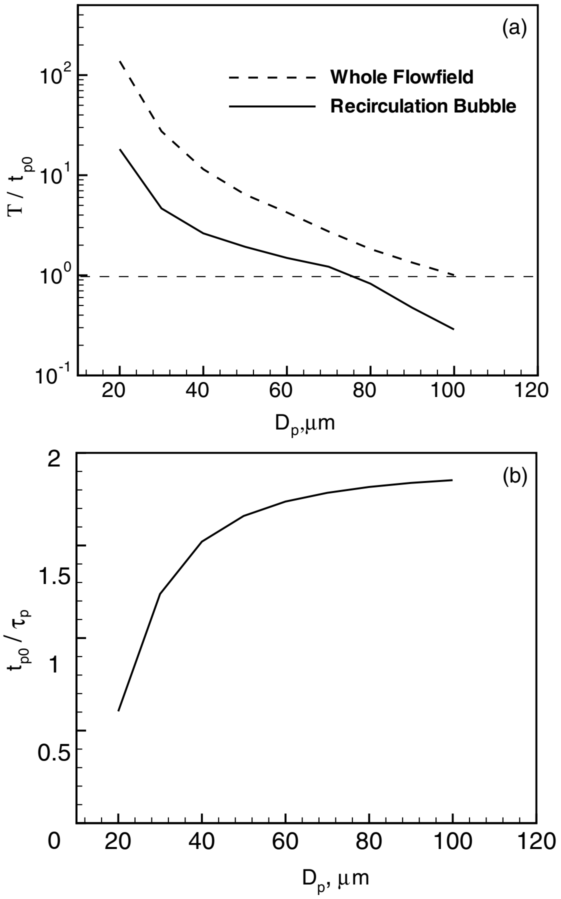

Fig. 11. Variation of residence-times with particle diameter: (a) — whole flowfield, - - - recirculation bubble, (b) t_{p0}/τ_p.

that these large particles do not come to rest within the recirculation bubble. Fig. 11b shows the variation of t_{p0} with the particle diameter. Here t_{p0} is normalized by the particle response time τ_p given in Eq. (5). Increasing t_{p0}/τ_p with diameter implies that bigger size particles travel longer distances in the axial direction before reversing their direction. Particles of sizes 75–80 μm penetrate the recirculation bubble entirely before reversing their direction as was shown in Fig. 9. These particles are then thrown towards the wall through swirling motion and escape the recirculation bubble, giving them the largest time to reside and interact with the reverse flow. Smaller particles ($d_p < 75$ μm) respond to the flow faster and are decelerated to zero axial velocity sooner. On the contrary, larger particles ($d_p > 80$ μm) do not come to halt within the recirculation bubble and also have small residence times.

3.3.4. Particle size-velocity correlations

The correlations between particle size and axial gas-phase velocity are shown in Fig. 12. These are in good agreement with the experimental values of Sommerfeld and Qiu (1991). Along the centerline, the velocity-diameter correlations show that the number of larger-size particles with negative velocities increases further downstream. At $x/R = 1.625$, small particles ($20 < d_p < 45$ μm) have negative velocities, while majority of larger particles have high positive velocity. This indicates that smaller particles have already reversed their direction, while heavier, large particles continue to penetrate the central recirculation zone. Further downstream, more particles in the

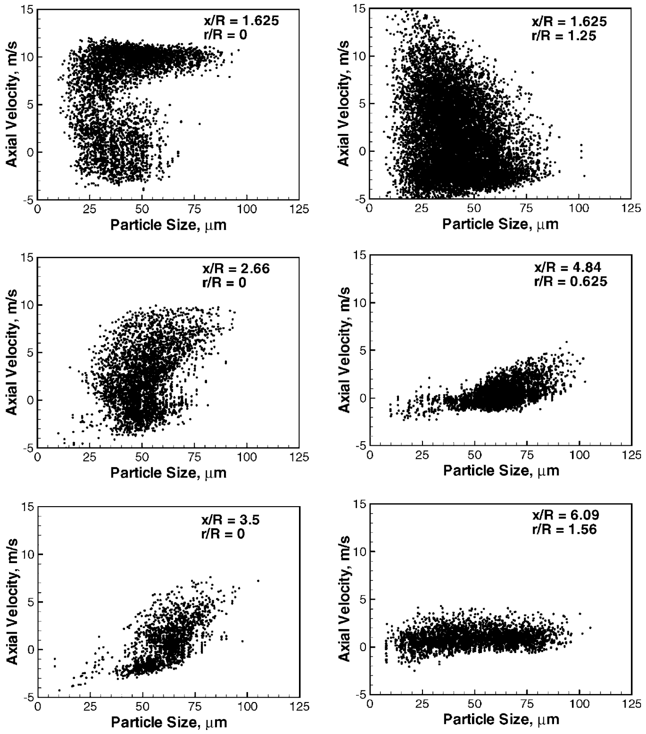

Fig. 12. Particle size-velocity correlations at different locations.

range ($50 < d_p < 80$ μm) have negative velocities while the number of small size particles close to the centerline has diminished. This indicates that the smaller size particles are thrown out of the recirculation zone by the swirling action, while large-scale particles are slowed down and continue to travel in the opposite direction. Further downstream, at $x/R = 4.8$ and $x/R = 6$, and away from the centerline, majority of the large-scale particles have positive velocities. There is an addition of small-scale particles with negative velocities in this region. This may correspond to the small size particles being re-trapped into the recirculation zone after getting reflected from the walls. The particle-velocity correlations are consistent with the mean number diameter distributions observed at various axial locations.

4. Summary

A LES of particle-laden, swirling flow in a coaxial-jet combustor is performed under conditions corresponding to an experiment by Sommerfeld and Qiu (1991). A mixture of air and lightly loaded, spherical, glass-particles with a prescribed size-distribution enters the primary jet, while a swirling stream of air flows through the annulus. The incompressible, spatially filtered Navier–Stokes equations are solved on unstructured grids to compute the turbulent gas-phase. A Lagrangian formulation and an efficient particle-tracking scheme on unstructured meshes is developed to compute the dispersed phase. The particles are treated as point sources and influence the gas phase (‘two-way’ coupling) only through momentum-exchange terms. To the best of our knowledge, the work described in this paper represents the first LES of turbulent particle-laden flows using a methodology that is directly applicable to complex engineering configurations.

Good agreement with experimental data is obtained for both phases. The LES results are significantly more accurate than the RANS predictions of the same problem (Sommerfeld et al., 1992). The success may be attributed to: (a) the effectiveness of LES in predicting turbulent mixing over RANS and (b) tracking of large number of particles to obtain a dynamic representation of the dispersed phase as opposed to the parcels-approach generally employed in RANS-based simulations. Particle dispersion characteristics are obtained by tracking approximately a million particles within the flowfield. The response of different size particles in the swirling flow is characterized by numerically estimating the residence times in the whole domain and within the central recirculation bubble. Additionally, particle trajectories obtained for different sizes show large differences in their evolution through the flowfield. Heavier particles with larger inertia rapidly penetrate the central recirculation bubble while smaller particles respond quickly to the rapid accelerations/decelerations of the gas-phase.

Acknowledgements

Support for this work was provided by the United States Department of Energy under the Accelerated Strategic Computing Initiative (ASCI), program. The computer resources provided on Blue Horizon at San Diego Supercomputing Center and ASCI Frost at Lawrence Livermore National Laboratory, CA are greatly appreciated. We would also like to thank Prof. Martin Sommerfeld for providing detailed experimental data in this configuration. We are indebted to Dr. G. Constantinescu and Mr. G. Iaccarino for their help at various stages of this study.

References

Crowe, C., Sommerfeld, M., Tsuji, Y., 1998. Multiphase Flows with Droplets and Particles. CRC Press, Boca Raton, FL.

Eaton, J.K., Fessler, J.R., 1994. Preferential concentration of particles by turbulence. Int. J. Mult. Flow. 20, 169–209.

Ferrante, A., Elghobashi, S.E., 2003. On the physical mechanisms of two-way coupling in particle-laden isotropic turbulence. Phys. Fluids 15, 315–329.

Germano, M., Piomelli, U., Moin, P., Cabot, W.H., 1991. A dynamic subgrid-scale eddy viscosity model. Phys. Fluids A 3, 1760–1765.

Kravchenko, A., Moin, P., 1997. On the effect of numerical errors in large-eddy simulation of turbulent flows in complex geometries. J. Comp. Phys. 131, 310–322.

Kulick, J.D., Fessler, J.R., Eaton, J.K., 1994. Particle response and turbulence modification in fully developed channel flow. J. Fluid Mech. 277, 109–134.

Lefebvre, A.H., 1989. Atomization and Sprays. Hemisphere, Washington, DC.

Li, G., Modest, M.F., 2001. An effective particle tracking scheme on structured/unstructured grids in hybrid finite volume/pdf Monte Carlo methods. J. Comp. Phys. 173, 187–207.

Lohner, R., 1995. Robust, vectorized search algorithms for interpolation on unstructured grids. J. Comp. Phys. 101, 307–313.

Mahesh, K., Constantinescu, G., Moin, P., 2000. Large-eddy simulation of gas turbine combustors. Annual Research Briefs, Center for Turbulence Research, Stanford University, pp. 219–228.

Mahesh, K., Constantinescu, G., Apte, S., Iaccarino, G., Moin, P., 2001. Large-eddy simulation of gas turbines combustors. Annual Research Briefs, Center for Turbulence Research, Stanford University, pp. 3–17.

Mahesh, K., Constantinescu, G., Moin, P., in preparation. A new time-accurate finite-volume fractional-step algorithm for prediction of turbulent flows on unstructured hybrid meshes. J. Comp. Phys.

Maxey, M.R., Patel, B.K., 2001. Localized force representations for particles sedimenting in Stokes flow. Int. J. Mult. Flow. 27, 1603–1626.

Maxey, M.R., Chang, E.J., Wang, L.-P., 1994. Simulation of interactions between microbubbles and turbulent flows. App. Mech. Rev. 47, S70–S74.

Mittal, R., Moin, P., 1997. Suitability of upwind-biased finite-difference schemes for large-eddy simulation. AIAA J. 35, 1415–1417.

Modest, M.F., 1993. Radiative Heat Transfer. In: McGraw-Hill Series in Mechanical Engineering. pp. 684–686.

Oefelein, J.C., 1999. Large eddy simulation of dilute particle-laden flows. In: ILASS Americas 12th Annual Conference on Liquid Atomization and Spray Systems, Indianapolis, IN.

Pierce, C., Moin, P., 1998. Method for generating equilibrium swirling inflow conditions. AIAA J. 36, 1325–1327.

Pierce, C., Moin, P., 2001. The progress variable approach for large eddy simulation of turbulent combustion, TF-Report 80, Flow Physics Division, Mechanical Engineering Department, Stanford University, Stanford, CA.

Sommerfeld, M., Qiu, H.H., 1991. Detailed measurements in a swirling particulate two-phase flow by a phase—doppler anemometer. Int. J. Heat and Fluid Flow 12, 20–28.

Sommerfeld, M., Qiu, H.H., 1993. Characterization of particle-laden, confined swirling flows by a phase—doppler anemometer. Int. J. Heat and Fluid Flow 19, 1093–1127.

Sommerfeld, M., Ando, A., Qiu, H.H., 1992. Swirling, particle-laden flows through a pipe expansion. J. Fluids Eng. 114, 648–656.

Westermann, T., 1992. Localization schemes in 2D boundary-fitted grids. J. Comp. Phys. 101, 307–313.